INVESTIGATION OF THE STRUCTURAL-PHASE STATE AND ITS ROLE IN THE FORMATION OF HEAT-RESISTANCE PROPERTIES OF 12% CHROMIUM STEEL

T. N. Vershinina, M. B. Ivanov, Yu. R. Kolobov, M. V. Leonteva-Smirnova, and Yu. F. Ivanov

UDC 539.4.016.3

Results of investigations into the structural-phase state of ÉK-181 ferritic-martensitic low-activate steel after thermal treatment including quenching, intermediate tempering, and subsequent long tempering under loading at temperatures of 923 and 973 K are presented. The influence of the defect substructure of the ferrite matrix, phase composition, and character of the secondary dispersed phase distribution in the volume of the material on the heat-resistant steel properties is examined.

INTRODUCTION

The necessity of increasing the heat resistance of ferritic-martensitic steels with high chromium content to expand the temperature range of their application in power engineering, including high-power nuclear reactors, makes a study of high-temperature (above 873 K) stability of their structural-phase state urgent. One of the examples of these steels is ÉK-181 (Fe–0.14C–11.2Cr–1.1W–0.29V–0.17Ta–0.007P) low-activate heat-resistant ferritic-martensitic steel produced at the All-Russian Scientific-Research Institute of Inorganic Materials [1–5] whose heat resistance increased (at temperatures higher than 873 K) due to the formation of martensite stabilized by second-phase particles.

The present article is a review of investigations into the structural-phase state and its influence on the heat-resistance properties of 12% chromium ferritic-martensitic low-activate steel.

MATERIAL AND EXPERIMENTAL PROCEDURE

The structure of ÉK-181 steel (Table 1) in states indicated in Table 2 was investigated by the methods of optical, scanning, and transmission electron microscopy and x-ray spectral microanalysis.

Investigations by the method of optical metallography were carried out with an Olympus GX71 microscope. Scanning electron microscopy (SEM) of chemically etched specimens and carbon replicas with particle extraction were carried out using Philips SEM 515 and Quanta 200 3D microscopes with accelerating voltage of 30 kV. The specimens were etched in an aqueous solution of hydrofluoric and nitric acids. The local element analysis of chemical composition of dispersed particles in the carbide phase precipitated on carbon replica was carried out by the method of energy dispersion microanalysis using an attachment to an EDAX IV Econ (PV9900) scanning electron microscope. Investigations by the method of transmission electron microscopy (TEM) of thin foils and replicas with particle extraction were performed using an ÉM-125 electron microscope with an accelerating voltage of 125 kV.

Belgorod State University, e-mail: Vershinina@bsu.edu.ru. Translated from Izvestiya Vysshikh Uchebnykh Zavedenii, Fizika, No. 11, pp. 36–42, November, 2007.

TABLE 1. Chemical Composition of ÉK-181 (Fe–0.14C–11.2Cr–1.1W–0.29V–0.17Ta–0.007P) Steel [1, 3] (Mass % with Fe as a Basis)

Steel	C	Cr	W	V	Ta	B	Si	Mn	P	S	N
ÉK-181	0.14	11.2	1.1	0.29	0.17	0.004	0.37	0.94	0.007	0.007	0.044

TABLE 2. Regimes of Thermal Treatment of ÉK-181 Steel

State	Regime of thermal treatment
1	Quenching from 1373 K
2	Quenching from 1373 K + tempering at 993 K for 3 h
3	Quenching from 1373 K + tempering at 993 K for 3 h + tempering at 923 K for 9657 h
4	Quenching from 1373 K + tempering at 993 K for 3 h + tempering under loading at 923 K for 9657 h
5	Quenching from 1373 K + tempering at 993 K for 3 h + tempering at 973 K for 733 h

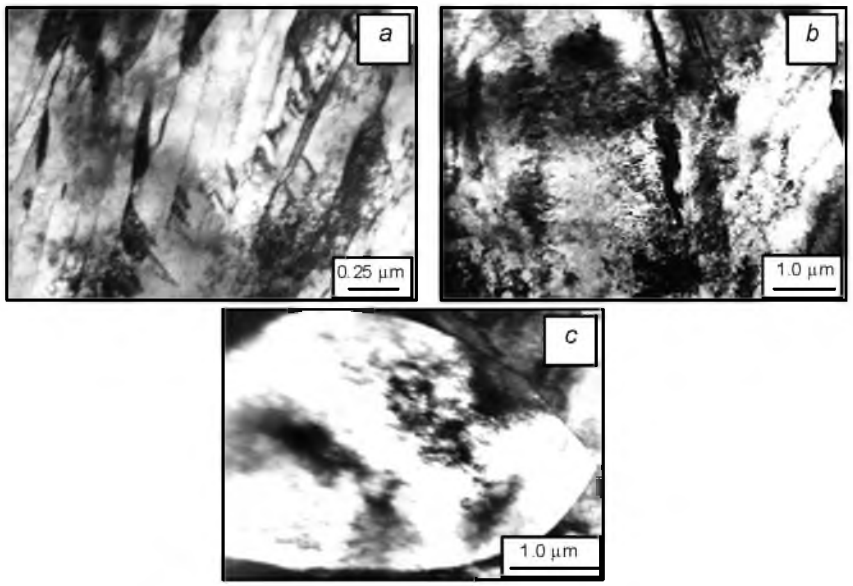

Fig. 1. Electron micrograph of the structure of Fe–0.14C–11.2Cr–1.1W–0.29V–0.17Ta–0.007P steel water-quenched from 1373 K: *a*) packet (lath) martensite, *b*) plate martensite, and *c*) δ-ferrite grain [3].

1. RESULTS OF INVESTIGATIONS

1.1. Structural-phase state of ÉK-181 steel after thermal treatment with quenching and subsequent tempering

After quenching from 1373 K, the structure comprising packet martensite crystals and high-temperature plate martensite with volume fractions of 80 and 20%, respectively (Fig. 1*a* and *b*), and ferrite grains with sizes of a few micrometers (Fig. 1*c*) was formed [3]. The average transverse sizes of packet martensite crystals in Fe–0.14C–11.2Cr–1.1W–0.29V–0.17Ta–0.007P steel tempered from 1373 K were $D = (200 \pm 10)$ nm; the transverse sizes of high-temperature plate martensite crystals changed in a wide range from 0.3 to 1.1 μm.

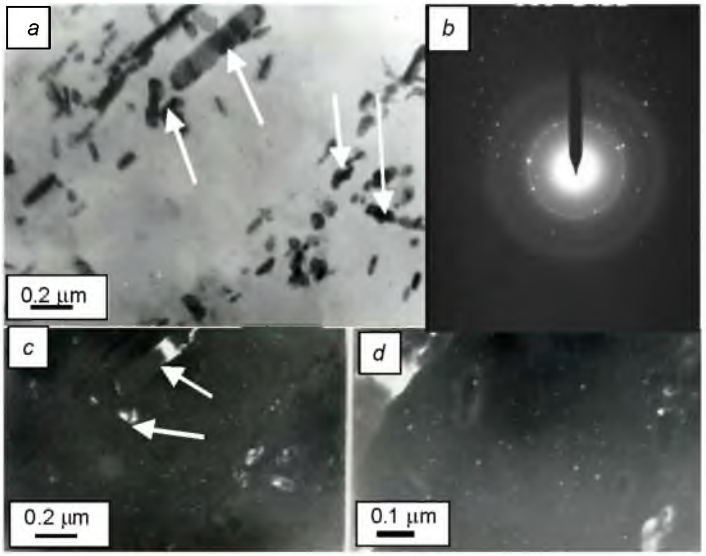

Fig. 2. Electron micrograph of the carbide phase particles formed in Fe–0.14C–11.2Cr–1.1W–0.29V–0.17Ta–0.007P steel thermally treated by quenching from 1373 K and tempering at 993 K for 3 h: *a*, *c*) $M_{23}C_6$ particles (indicated by arrows), and *b*) electron diffraction pattern to (*a*). The method of carbon replica with carbide phase extraction [5] was used.

Tempering of quenched steel at 993 K for 3 h led to the initial recrystallization stages. Two mechanisms of this process were revealed [3]. One of them, characteristic of packet martensite, involved a scatter of low-angle crystal boundaries. We note that the given mechanism is similar to the mechanism of paired coalescence frequently observed during recrystallization of the deformed metals and alloys accompanied by low degrees of subgrain misorientation [6]. Another mechanism of martensitic steel fracture is realized by means of nucleation and subsequent growth of recrystallization centers localized in grain joints and martensite packets and plates. As demonstrated in [7, 8], this mechanism was characteristic of severely deformed metals and alloys with high degrees of misorientation of the boundaries.

As demonstrated investigations performed by the TEM method, the scalar density of dislocations inside the martensitic crystals in volumes of the material that retained the morphology of quenching structure decreased after tempering by a factor of 1.5–2 [3, 5]. The relaxation of dislocation substructures was accompanied by fragmentation of the martensitic crystals. Fragments, as a rule, were anisotropic, and the azimuth component of the total misorientation angle revealed by an analysis of electron micrographs was $\Delta\alpha \sim 4$–5 deg [9].

Tempering of Fe–0.14C–11.2Cr–1.1W–0.29V–0.17Ta–0.007P steel is accompanied by the transformation of the carbide phase particles, which involves dissolution of self-tempered cementite particles and precipitation of special carbide particles. The main of them are chromium-based $M_{23}C_6$ carbide particles and MX (where M denotes atoms of the carbide-forming element and X denotes C or N atoms) carbonitride particles. The $M_{23}C_6$ carbide particles are mainly localized on intraphase boundaries and have globular shapes (Fig. 2*a* and *c*); the vanadium carbide (carbonitride) particles, localized on the intraphase boundaries, can also be shaped as thin interlayers whose transverse sizes do not exceed 40 nm [3]. Vanadium carbonitride precipitates were also detected in packet and plate martensite crystal volume on dislocations (Fig. 2*d*). The particles had spherical shapes, and their sizes were 3–5 nm.

In addition to the main carbides ($M_{23}C_6$) and carbonitrides (MX), an insignificant amount of chromium-based Cr_7C_3, Cr_3C_2, and M_6C carbides were observed in Fe–0.14C–11.2Cr–1.1W–0.29V–0.17Ta–0.007P steel. These carbide particles were mainly localized along the intraphase boundaries and had globular shapes with average particle sizes of 40 nm. The Laves Fe_2W phase particles were detected along the δ-ferrite grain boundaries.

Size distributions of secondary-phase particles constructed from dark-field TEM images of steel microstructure (Fig. 3*a*) and SEM images of the structure of etched crystallographic specimens (Fig. 3*b*) allow us to judge about an ensemble of particles as a whole. The examined particles were mainly localized on the martensite crystal boundaries and

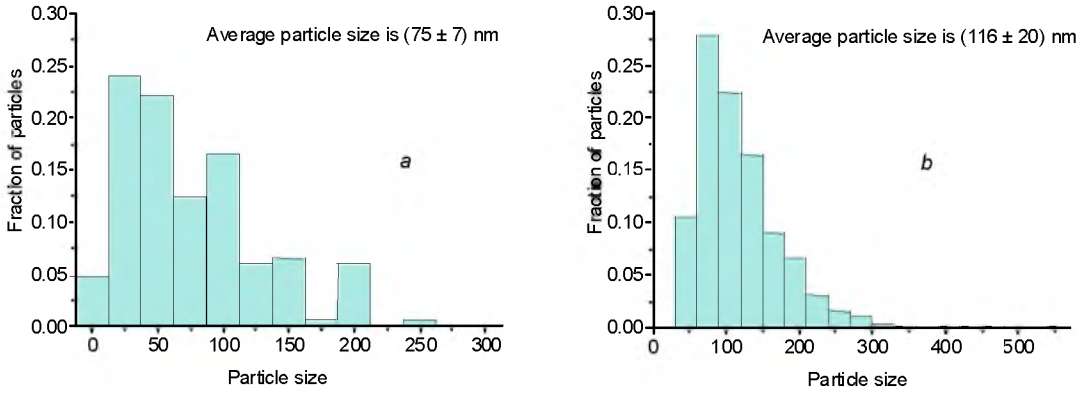

Fig. 3. Histograms of the second-phase particle sizes in Fe–0.14C–11.2Cr–1.1W–0.29V–0.17Ta–0.007P steel obtained by an analysis of dark-field TEM (*a*) and SEM microstructure images (*b*).

subboundaries and had anisotropic shapes. As a consequence, the longitudinal and transverse particle sizes were measured, and the average size was determined and filed into the database used for histogram construction. The difference between histograms obtained by the TEM and SEM methods was due to the possibility of consideration of large (larger than 300 nm) and impossibility of consideration of fine (smaller than 30 nm) precipitates when analyzing images of crystallographic specimens by the SEM method. However, a phase analysis of carbon replicas with particle extraction performed by the method of transmission electron microscopy with the use of the same etcher as for the construction of SEM images demonstrated the presence of a spectrum of carbide precipitates similar to those observed in the process of TEM of thin foils. Hence, the size distributions of the second phases recorded by the SEM method reflect the true structural-phase state of steel with limitations on particles with sizes less than 30 nm, and the given method can be used for an express analysis of second-phase inclusions.

We succeeded in performing a qualitative analysis of the alloying element content in individual second-phase particles which sizes no smaller than 0.2 μm by the methods of SEM and energy dispersion microanalysis applied to carbon replicas with particle extraction. It was revealed that in Fe–0.14C–11.2Cr–1.1W–0.29V–0.17Ta–0.007P steel quenched from 1373 K and tempered at 993 K for 3 h, most particles comprised chromium and iron (in the ratio Cr: Fe ~ 2: 1), which corresponded to the $M_{23}C_6$ phase according to the data of diffraction analysis by the TEM method. In this case, the $M_{23}C_6$ phase was slightly alloyed by W (with atomic fraction no more than 10% of the metal fraction of particles).

1.2. Influence of the structural-phase state on heat-resistant properties of 12% chromium steels

A study of laws and mechanisms of high-temperature deformation of Fe–0.14C–11.2Cr–1.1W–0.29V–0.17Ta–0.007P steel revealed a high level of mechanical properties at temperatures up to 923 K and their decrease at 973 K [5]. One of the factors determining the high level of mechanical properties is the formation of a stable dispersed structure of the ferrite matrix retaining the morphology of packet martensite during thermal treatment (quenching from 1373 K and tempering at 973 K for 3 h). At the same time, as indicated above, the martensitic transformation into Fe–0.14C–11.2Cr–1.1W–0.29V–0.17Ta–0.007P steel is accompanied by the formation of packet (lath) martensite (with volume fraction of ~80%) and high-temperature plate martensite (~20% of the volume). It is well known that the volume fraction of coarsely-dispersed plate martensite can be decreased by decreasing austenite grain sizes; however, according to some data, this should result in the formation of unstructured martensite [10] that does not provide an increase in the mechanical properties.

One of the parameters of long-term thermal stability of examined steel at temperatures up to 923 K is suppression of the α-phase recrystallization processes [3]. Investigations by the TEM method demonstrated that, despite repeated tempering at 923 K for 9657 h, the α-phase structure retained the morphology preset by quenching, namely, in most cases the α-phase had the shape of martensitic crystals. Inside the α-phase crystals, a dislocation network substructure was observed with scalar dislocation density of approximately $2.5 \cdot 10^{10}$ cm^2. Tempering of steel was accompanied by the initial

stages of recrystallization process. As in the case of intermediate tempering, the following recrystallization processes were observed: the scatter of α-phase crystal boundaries, formation of grain and subgrain packets in joints, and formation of subgrain structures along the boundaries of δ-ferrite grains. As demonstrated investigations by the methods of electron microscopy, the main reason for thermal and mechanical stabilities of the steel structure is precipitation of dispersed carbide globular ($M_{23}C_6$) and plate (MX) phases on the martensite crystal boundaries and finely dispersed (3–5 nm) MX carbonitrides in martensite crystal volumes during tempering in the preparatory stage (preliminary tempering at 993 K for 3 h) [5]. The latter is the main reason for suppression of initial steel recrystallization during superlong-term holding at temperatures of 923 K.

The well-known models allow the influence of second-phase particles on the recrystallization process to be elucidated [11, 12]. Particles move together with boundaries under condition that

$$f_r \geq f_b, \tag{1}$$

where $f_b = 2\gamma_s / \overline{D_s}$ is the driving force of boundary migration, $f_r = 3\gamma_b \nu / \overline{d}$ is the force of particle resistance to migration, γ_s is the surface energy of the subboundary, γ_b is the surface energy of the large-angle interphase boundary, ν is the volume fraction of particles, $\overline{D}_s$ is the average subgrain size, and $\overline{d}$ is the average particle size. In this case,

$$\gamma_s = \gamma_b \frac{\theta_m}{\theta_{max}}\left(1 - \ln\frac{\theta_m}{\theta_{max}}\right), \tag{2}$$

where θ_m is the misorientation angle of the low-angle boundary, θ_{max} is the maximum misorientation angle of the low-angle boundary which shows the properties of the large-angle boundary.

Substitution of the corresponding values for the average energy of low-angle boundaries set equal to 0.3 of the energy of the large-angle boundary, the volume fraction of particles set equal to 2–3%, average subgrain size of ~0.2 μm, and average particle size of 0.1 μm allows us to conclude that the driving recrystallization force exceeds several times the force of particle resistance to the boundary motion. However, it should be noted that the preferable arrangement of particles on the subboundaries increases several times their effective volume fraction that must be used in calculations. In addition, the boundary surface area replaced by a particle considerably exceeds the area calculated in the approximation of spherical particles due to a high degree of particle anisotropy. This is especially clearly seen on the example of vanadium carbides (particle sizes ~60 × 130 nm). Consideration of these factors in our calculations results in equality of the driving recrystallization force and the force of second-phase particle resistance to the migration of boundaries.

After long-term creep at 923 K for 9657 h, the carbide sizes increased insignificantly (their average size was (239 ± 30) nm); therefore, even after long-term annealing, the condition of particle migration together with the grain boundaries can be fulfilled.

Thus, after long-term annealing, the second-phase particles effectively hinder the migration of boundaries, and the driving force of primary recrystallization during static annealing appears insufficient for the separation of boundaries from the carbide precipitates. Hence, the main recrystallization mechanism of examined steel is the paired coalescence of adjacent packet martensite crystals with low-angle misorientation.

Proceeding from the aforesaid, we can conclude that one of the most important parameters determining the structural stability of packet martensite in Fe–0.14C–11.2Cr–1.1W–0.29V–0.17Ta–0.007P steel during high-temperature tempering is the fraction of low-angle boundaries in the packet. In this regard, on the example of steel tempered from 1373 K and steel subjected to tempering at 993 K for 3 h and subsequent repeated tempering at 923 K for 733 h (region of fractured specimen capture for long operating lifetime tests), we investigated the thermal stability of martensitic structures, determined the ratio of large- to low-angle boundaries in the packet, and considered mechanisms of defect matrix substructure degradation.

By the TEM methods, it was established that in the capture zone of the specimen subjected to long-term (733 h) tempering at 973 K, the α-phase structure was observed that retained the martensite morphology and defect substructure in different degrees. By the morphological parameter, uniform and non-uniform packets were classified. The transverse packet

martensite crystal sizes averaged over the volume of the material were $D = (0.47 \pm 0.02)$ μm. In addition, areas of α-phase without intraphase boundaries were observed with sizes of ~3–20 μm. Their volume fraction was small (~10%). The density of dislocations chaotically distributed in these areas was $\sim 1.5 \cdot 10^{10}$ cm^2. Carbide-phase particles, sometimes arranged in series, were observed inside α-phase regions. This suggests that these areas were formed as a result of scatter of low-angle boundaries of packet martensite crystals and were not caused by the recrystallization processes that occurred by means of migration of boundaries.

Uniform packet martensite was characterized by crystals having close values of transverse sizes. The volume fraction of the martensite packets was ~30%. The average transverse sizes of the martensite crystals were $D = (0.28 \pm 0.010)$ μm, which was slightly greater than the average transverse sizes of the martensite crystals in tempered steel. The revealed difference between the transverse sizes of packet martensite crystals in tempered steel and of the capture zone demonstrate that paired coalescence accompanied by a scatter of the boundaries between the neighboring martensite crystals can be observed in these packets in separate cases.

The non-uniform packets are characterized by transverse sizes of martensite crystals that differ by an order of magnitude. The volume fraction of these packets is ~60%. The average transverse sizes of martensite crystals in them are $D = (0.55 \pm 0.02)$ μm, which is much greater than the average transverse sizes of martensite crystals in tempered steel. Hence, during thermal treatment, the most part of martensite crystals was fractured by means of scatter of the boundaries dividing them.

Comparing the above-discussed average transverse sizes of the packet martensite crystals in annealed and tempered states, we can conclude that the ratio of large- to low-angle boundaries dividing the martensitic crystals is 1: 1.

To present the results obtained in a natural way, we choose the parameter $\beta = C/\mathrm{Me}$, where C is the total concentration of interstitial atoms (carbon and nitrogen), and Me is the total concentration of substitution atoms (nickel, chromium, and manganese). This parameter describes a degree of relative iron alloying. As shown in [13], an increase in the parameter β is accompanied by an increased degree of misorientation of the packet structure: from mostly low-angle misorientation of laths to mostly large-angle misorientation and increase in the number of martensite crystals with large-angle misorientation in the packet.

This approach to investigation of Fe–0.14C–11.2Cr–1.1W–0.29V–0.17Ta–0.007P steel allowed us to calculate the parameter β which was $\sim 12 \cdot 10^{-3}$. It then follows that packet martensite with dominant large-angle lath misorientation should be formed in examined steel. This approach well describes the original experimental facts, in particular, the estimated ratio of large- to low-angle boundaries in the packet equal to 1:1.

Fe–0.14C–11.2Cr–1.1W–0.29V–0.17Ta–0.007P steel is a dispersion-hardening alloy [5]. This is testified by the fact that even after long-term annealing, the process of polygonization of the martensitic structures is not completed, and unusually high density of chaotically arranged dislocations is retained. Thus, the annealing dislocation density in steel equal to $\sim 10^{11}$ cm^2 decreases insignificantly (to $\sim (3–4) \cdot 10^{10}$ cm^2) during high-temperature stabilizing tempering (at 993 K for 3 h). During subsequent long-term annealing (at temperatures up to 923 K for more than 700 h), the dislocation density remained virtually unchanged; moreover, significant stresses were retained inside the packet volume. They were detected by the TEM method. Obviously, stabilization of the dislocation substructure is caused by precipitation of finely-dispersed vanadium carbonitride particles with sizes of 3–5 nm inside martensite crystal volumes. Vanadium carbonitrides were also observed as plates precipitated on the intraphase boundaries stabilizing them. It is particularly remarkable that the average sizes of vanadium carbide particles remained virtually unchanged under conditions of long-term tempering at temperatures up to 973 K. It is well known [14] that these particles in chromium steels are precipitated from the supersaturated solid solution at temperatures above 873 K and retain their dispersiveness up to temperatures of about 1023 K.

CONCLUSIONS

We have been investigated the phase structure and defect substructure of Fe–0.14C–11.2Cr–1.1W–0.29V–0.17Ta–0.007P steel subjected to quenching and intermediate and subsequent long-term high-temperature tempering.

It was established that the main factor determining the high thermal stability of Fe–0.14C–11.2Cr–1.1W–0.29V–0.17Ta–0.007P steel was optimal microalloying by carbide- and nitride-forming elements that allowed quenching and subsequent dispersion hardening stabilizing the defect substructure of the material.

Estimates were obtained and it was demonstrated that the carbide phase particles localized on the martensite crystal boundaries were the efficient structure stabilizers suppressing the recrystallization processes occurring by the mechanism of migration of large-angle boundaries.

It was established that the formation of recrystallization centers at temperatures up to 973 K occured by the mechanism of coalescence of packet martensite crystals by means of scatter of the low-angle boundaries. The assumption was made that the additional factor determining the thermal stability of steel could be the relative content of large-angle boundaries subdividing the martensite crystals.

This work was done on the equipment of the Center of Nanostructural Materials and Nanotechnologies – Multiaccess Center at Belgorod State University. This work was supported in part by the Federal Goal-Oriented Program (grant No. 02.552.11.7017).

REFERENCES

1. A. G. Ioltukhovskiy, M. V. Leonteva-Smirnova, M. I. Solonin, *et al.*, J. Nucl. Mater., **307–311**, 532–535 (2002).
2. M. V. Leonteva-Smirnova, A. G. Ioltukhovskiy, G. A. Arutiunova., *et al.*, J. Nucl. Mater., **307–311**, 466–470 (2002).
3. M. V. Leonteva-Smirnova, A. G. Ioltukhovskiy, V. M. Chernov, *et al.*, Vopr. Atomn. Nauki Tekh., Ser. Materialoved. Nov. Mater., No. 2 (63), 142–155 (2004).
4. Yu. R. Kolobov, E. V. Naidenkin, M. B. Ivanov, *et al.*, Vopr. Atomn. Nauki Tekh., Ser. Materialoved. Nov. Mater., No. 2 (63), 156–162 (2004).
5. M. V. Leonteva-Smirnova, A. N. Agafonov, G. N. Ermolaev, *et al.*, Perspekt. Mater., No. 6, 40–52 (2006).
6. L. N. Larikov and E. E. Zasimchuk, in: Studying Defects of the Crystal Structure in Metals and Alloys [in Russian], Naukova Dumka, Kiev (1966), pp. 70–84.
7. S. S. Gorelik, Recrystallization of Metals and Alloys [in Russian], Metallurgiya, Moscow (1978).
8. F. Hessner, ed., Recrystallization of Metal Materials [in Russian], Metallurgiya, Moscow (1982).
9. L. M. Utevskii, Electron Diffraction Microscopy in Metal Research [in Russian], Metallurgiya, Moscow (1973).
10. G. V. Kurdyumov, L. M. Utevskii, and R. I. Éntin, Transformations in Iron and Steel [in Russian], Nauka, Moscow (1977).
11. R. O. Caen and P. Haazen, eds., Physical Metallurgy, Vol. 3. Physicomechanical Properties of Metals and Alloys [Russian translation], Metallurgiya, Moscow (1987).
12. Yu. R. Kolobov, Diffusion-Controllable Processes on Grain Boundaries and Plasticity of Metal Polycrystals [in Russian], Nauka, Novosibirsk (1998).
13. Yu. F. Ivanov, Izv. Vyssh. Uchebn. Zaved., Chern. Metallurg., No. 10, 52–54 (1995).
14. K. A. Lanskaya, High-Chromium High-Resistant Steels [in Russian], Metallurgiya, Moscow (1976).